IEEE Access
Multidisciplinary | Rapid Review | Open Access Journal

Received March 17, 2020, accepted April 1, 2020, date of publication April 3, 2020, date of current version April 21, 2020.

Digital Object Identifier 10.1109/ACCESS.2020.2985505

Interferometric SAR Phase Filtering With SURE-Based Non-Local Method

RUI GUO[1], BO ZANG[2], SHUANG-XI ZHANG[3], (Member, IEEE), AND MENG-DAO XING[2], (Member, IEEE)

[1]School of Automation, Northwestern Polytechnical University, Xi'an 710129, China
[2]School of Electronic Engineering, Xidian University, Xi'an 710071, China
[3]School of Electronics and Information, Northwestern Polytechnical University, Xi'an 710129, China

Corresponding author: Rui Guo (gr2003@nwpu.edu.cn)

This work was supported in part by the National Natural Science Foundation of China under Grant 61701410 and Grant 61701374, and in part by the Natural Science Basic Research Plan in Shaanxi Province of China under Grant 2019JQ-418.

ABSTRACT As the phase of the interferometric synthetic aperture radar (InSAR) contains abundant information for many earth observation activities, the interferometric phase denoising is an important step before InSAR processing and application because of its significant influence on the following steps. And this paper focused on the interferometic phase filtering and proposed a new filter based on the Stein's unbiased risk estimate (SURE)-based nonlocal means method. The SURE formula is more convenient for estimating the mean square error (MSE) from the noisy image only. Due to advantages of both the nonlocal means and the Stein's unbiased risk estimate, the proposed filter is exploited to the interferometric phase in the complex domain in the paper. Except for the denoising performance, the proposed method is more focused on preserving more useful information in the InSAR phase fringe patterns, such as the phase jumps utilized for urban information retrieval. The experiments on both the simulated data sets and the real data sets were implemented and analyzed to demonstrate the effectiveness of the proposed filtering method.

INDEX TERMS Interferometric synthetic aperture radar (InSAR), interferometric phase filtering, Stein's unbiased risk estimate (SURE)-based nonlocal means.

I. INTRODUCTION

The rapid developed synthetic aperture radar (SAR) techniques, especially the high-resolution interferometric SAR (InSAR) make it possible to observe more detail information of the targets in many remote sensing activities. Herein, the interferometric phase shows its great power in many InSAR remote sensing applications [1]–[3]. However, the existence of the noise in the InSAR phase which introduced by several factors, such as thermal noise, different decorrelation, SAR image coregistration, will affect the InSAR data processing and following application. Hence, InSAR phase noise filtering as a curial step is inevitable to reduce the number of residues (NOR) in the interferogram, and various methods are proposed to filter the noise.

Till now, except for a typical group of methods that simultaneously filter and unwrap the interferometric phase [4], [5], many proposed InSAR filtering methods are structured on the models involving the reflectivity, coherence and phase together, such as the classical Lee filter [6] which presented an adaptive model using directional mask. Still, there are some other methods that only aim at the interferometric phase and construct the filtering model in different domain by using simple or comprehensive methodologies [7], [8]. Considering the related amount of data in the filtering process, these filtering methods dealing with only the phase usually should have much higher operating efficiency than those handling the reflectivity-coherence-phase involved model. Meanwhile, it could reduce the effects of reflectivity and coherence on the phase filtering, which only depends on the internal information of the interferometric phase itself [9]–[11]. Nowadays not only the unwrapped phase but also the wrapped phase has already been utilized for remote sensing applications [3], [12], so more convenient filter should be studied for only InSAR phase image to preserve more useful information contained in the phase.

As known, noise filtering is usually at the cost of image resolution, and nonlocal means is introduced for resolving

The associate editor coordinating the review of this manuscript and approving it for publication was Junjie Wu.

this problem caused by the general local means [13]–[16]. Compared with the local methods, nonlocal methods take the advantages of the patch-base processing. Because the nonlocal filtering methods can keep the details much better, it has been widely used in many types of images including the InSAR interferogram [1], [16], [17]. Herein, Deledalle *et al.* proposed the nonlocal interferogram estimation scheme called NL-InSAR filter [15], which has been widely taken as reference in many other researches [1], [8]. Based on the patch similarity criterion with reflectivity-coherence-phase involved model, a weighted maximum likelihood estimation of the InSAR interferogram was introduced, and the joint estimation of the reflectivity, interferometric phase and coherence was achieved but showed a tendency of oversmoothing [1]. In other words, it will cause the loss of structure detail such as the edges of phase fringes.

As Stein's unbiased risk estimate (SURE) can monitor the mean square error (MSE) of nonlocal means [18], [19] without noise free prior knowledge, SURE-based nonlocal means has already been suggested for image denoising [14], [15], which takes the advantages of both the nonlocal means the Stein's unbiased risk estimate. Motivated by the efficiency and better performance of the SURE-based nonlocal means, the proposed method based on the SURE-based nonlocal means is introduced for InSAR phase filtering in complex domain. The prior capability of the method is shown by preserving the phase patterns and keeping more texture details while reducing the noise.

In the rest of the paper, the background theory about SURE-based nonlocal means is firstly introduced in Section II. Then the InSAR filtering method is proposed and described based on the SURE-based nonlocal means in Section III. In Section IV, different data sets, including two simulated data sets and two real data sets, are used to evaluate the robustness of the filtering method. Experimental results show the effectiveness of this method by comparing with other classical filters.

II. PRINCIPLES OF SURE-BASED NONLOCAL MEANS

SURE is proposed without having a noise free prior knowledge to reach an unbiased estimate of MSE for the following observation model

$$y(i) = x(i) + n(i) \tag{1}$$

where x is the noise-free image, n stands for zero-mean white Gaussian noise with variance σ^2 and y is the measured noisy data. i denotes the ith pixel in the image.

The MSE of the denoised image with respect to the noise-free image is

$$\mathrm{MSE}_0 = \frac{1}{N}\left\|x - \hat{x}\right\|^2 \tag{2}$$

where $\|\cdot\|^2$ is Euclidean norm and N denotes the total number of the pixels. $\hat{x}$ is the denoised image.

SURE provides a means for unbiased estimation of the MSE without the noise-free image. And SURE-based nonlocal means is obtained as

$$\mathrm{SURE} = \frac{1}{N}\left\|y - \hat{x}\right\|^2 - \sigma^2 + \sigma^2\frac{\partial\hat{x}}{\partial y} \tag{3}$$

where $\hat{x}$ refers to the estimated result by nonlocal means. $\frac{\partial\hat{x}}{\partial y}$ is the divergence of the output estimate from the measurements For the ith pixel, the equation can be expressed as

$$\mathrm{SURE}(i) = \frac{1}{N}\left[y(i) - \hat{x}(i)\right]^2 - \frac{\sigma^2}{N} + \frac{2\sigma^2}{N}\frac{\partial\hat{x}(i)}{\partial y(i)} \tag{4}$$

and the nonlocal means output estimate $\hat{x}(i)$ is

$$\hat{x}(i) = \sum_{i\in\Omega(i)}\frac{\omega(i,j)y(j)}{\sum_{j\in\Omega(i)}\omega(i,j)} \tag{5}$$

where $\Omega(i)$ is the neighborhood used and $\omega(i,j)$ is the nonlocal weight computed by patches centered on pixels i and j as

$$\omega(i,j) = \exp\left(-\frac{\sum_{k\in K}\left(y(i+k) - y(j+k)\right)^2}{2Bh^2}\right) \tag{6}$$

where h is the nonlocal filtering parameter. B and K depend on the patch size for the nonlocal means. For example, if the patch size is 7×7, $B = 49$ and $K = [-3:3, -3:3]$.

The divergence term in (4) is defined as

$$\begin{aligned}\frac{\partial\hat{x}(i)}{\partial y(i)} = {} & \frac{\widehat{x^2}(i) - \hat{x}^2(i)}{Bh^2} + \frac{1}{W(i)} \\ & + \frac{1}{Bh^2W(i)}\sum_{k\in K}\omega(i-k)\left(y(i) - y(i+k)\right) \\ & \left(\hat{x}(i) - y(i-k)\right)\end{aligned} \tag{7}$$

where $W(i) = \sum_{j\in\Omega(i)}\omega(i,j)$.

It is noted in (3) that SURE relates to the estimated σ^2. Meanwhile, the nonlocal means performance depends on the nonlocal filtering parameter h. Hence, h is set according to the estimated σ^2. In practice, the optimal h could be found by combing SURE in (4) with an optimization strategy in a few iterations [15].

III. SURE-BASED NONLOCAL InSAR FILTER

A. MODEL OF THE NOISY INSAR PHASE

The interferometric SAR phase can be considered with the additive noise model:

$$\varphi = \alpha + n \tag{8}$$

where φ is the measured noisy InSAR phase, α is the ideal phase without noise and n is the additive noise with a zero mean and standard deviation. α and n are independent of each other. As the InSAR phase occurs in the interval of $[-\pi, \pi]$, the direct filtering in the real domain cannot be applied because of the phase jumps, where the phase value goes from $-\pi$ to π or π to $-\pi$. However, the phase jumps, such as the wrapped phase patterns, should be preserved in order to correctly retrieve the target information.

As the InSAR phase in the complex domain is continuous [20], the phase is considered to be processed in this domain to preserve the fringe patterns. And the phase noise model in the complex domain can be expressed as follows:

$$\cos(\varphi) = N_c \cos(\alpha) + n_r \tag{9}$$

$$\sin(\varphi) = N_c \sin(\alpha) + n_i \tag{10}$$

Equation (9) and (10) are the real and imaginary parts of the complex InSAR phase, respectively. n_r and n_i are zero-mean additive noise. N_c is the InSAR phase quality indicator. According to this model, both the real part and imaginary are filtered, and then the final filtered phase is composed by these two parts.

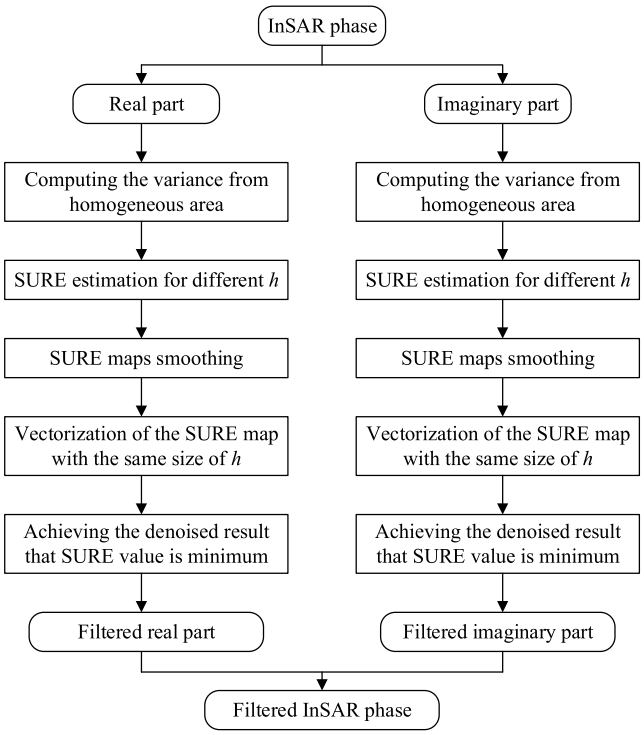

FIGURE 1. General flowchart of the proposed filtering method.

B. SURE-BASED NONLOCAL InSAR PHASE FILTERING METHOD

Figure 1 shows the flowchart of the SURE-based nonlocal InSAR phase filtering. Firstly, the InSAR phase is separated into the real part and the imaginary part according to Equation (9) and (10). Then, for both the real and imaginary parts, the SURE-based nonlocal filtering is implemented. Finally, the filtering phase is get from the filtered real and imaginary parts. In the filtering process, detailed steps still remain to be discussed.

The filtering steps are the same for both the real part and the imaginary part, and are as follows.

Step 1: As the SURE value is related to the variance σ^2, the variance σ^2 is calculated after separating the InSAR phase into real and imaginary parts. As usually it is unable to distinguish the noisy region from the textured region in the image, the estimated local variance from some pixels are not robust due to the inferior gradient measure.

To estimate the variance value, the pixels in the homogeneous area are selected using the threshold determination method referred to the former work in [21]. The similarity value used in (6) are calculated for different regions, such as noisy region and textured region. Then the probability density functions (PDF) of these similarity values are achieved. Comparing the two PDF, the threshold is set as the intersection of the two PDFs. Hence, the variance σ^2 is computed from the homogeneous area instead of a local window.

Step 2: Instead of a fixed filtering parameter h in (7), different filtering parameters are adopted.

According to Equation (4)-(7), SURE is computed in core of nonlocal means. As suggested in [22], the phase image is denoised by nonlocal means with different filtering parameters such as $h = \sigma^2 \times [0.3 : 0.005 : 0.35]$.

Step 3: From above, different SURE estimations can be obtained with different filtering results/denoised images due to different filtering parameter h. As a result each denosied image can produce a SURE map. The size of h is the number of SURE maps.

To achieve robust results, every SURE map is smoothed by convolving with locally adaptive regression kernels. As abovementioned in *Step 1*, for the pixels in homogeneous area, the flat smoothing kernel is used. On the contrary, the smoothing kernel will be ignored for the heterogeneous pixels.

Step 4: For each pixel in the denoised image, its SURE values are picked up from all the SURE maps, and then the SURE values of each pixel is set to form a vector with the same size of h.

Step 5: From the constructed vector composed by different SURE values of the ith pixel, the minimum SURE value is selected, and then the corresponding denoised result is taken as the best filtered result of the ith pixel.

After that, the best filtered result of all the pixels are obtained.

IV. EXPERIMENTS AND RESULTS

In this section, the performance of the proposed filtering method is investigated on both the simulated data sets and the real data sets of urban area. Two other filters including the classical Goldstein filter and the typical NL-InSAR filter are used for comparison. The window size of Goldstein filter is set as 12×12 for the simulated data sets and 10×10 for the real urban data sets with $\alpha = 0.5$. The parameters of NL-InSAR filter is as follows: a minimum equivalent number of looks of 10 and a number of iterations of 10; for simulated data sets, the search window size and the patch window size of NL-InSAR filter are 21×21 and 7×7, respectively; for real data sets, the search window size and the patch window size are the default values 15×15 and 5×5. The search window size and the patch window size of the SURE-based nonlocal InSAR phase filtering method are the same as the NL-InSAR

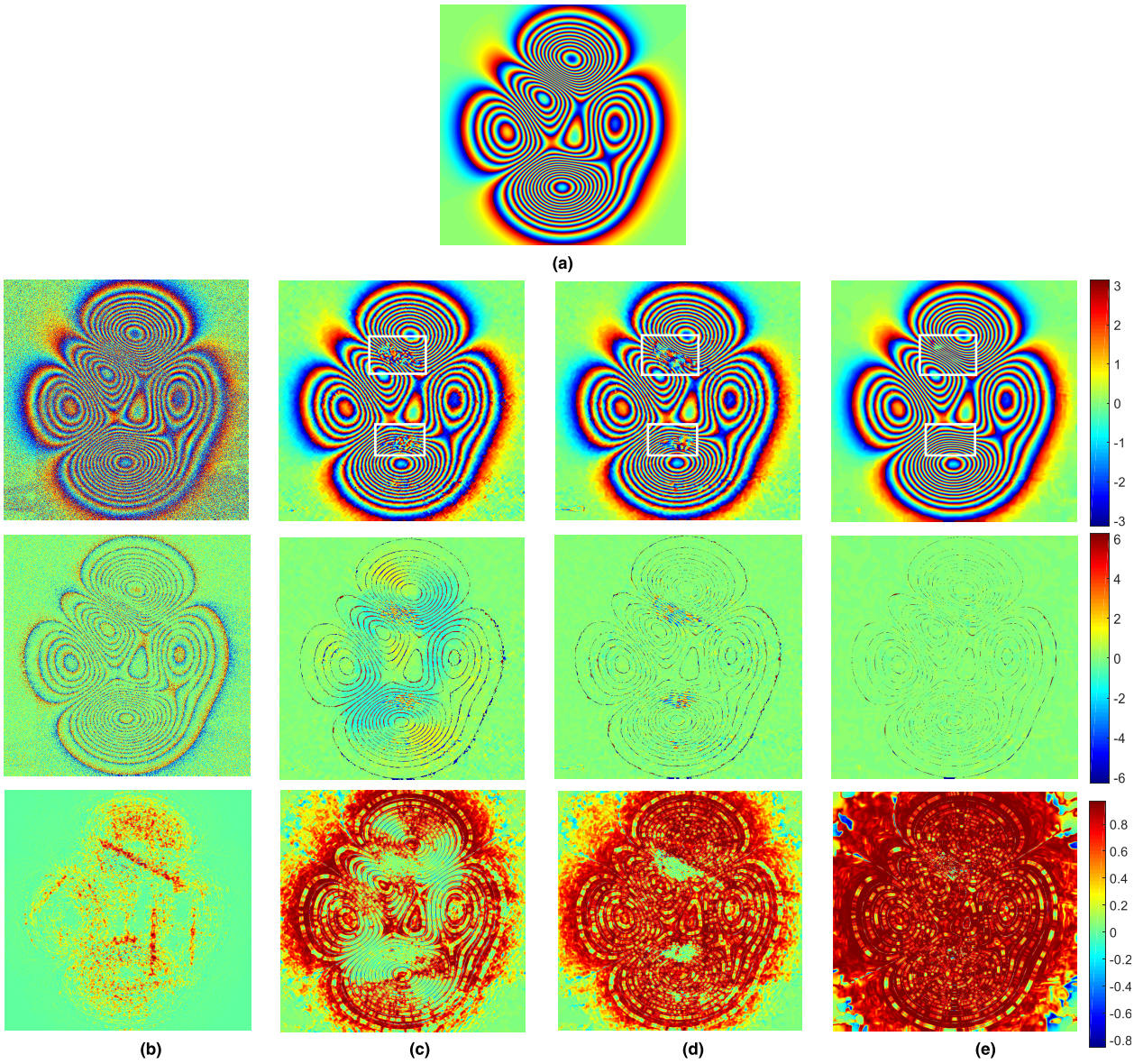

FIGURE 2. (a) Simulated ideal phase. Second row: filtered phase; Third row: phase difference to the ideal phase; Last row: SSIM map. (b) Noisy phase. (c) Goldstein filtered phase. (d) NL-InSAR filtered phase. (e) Filtered phase using the improved SURE-based nonlocal method.

filter used. All the experiments were performed on a PC with 2.90 GHz Intel Core CPU and 16 GB memory.

A. SIMULATED DATA

The InSAR phase of the first simulated data set is shown in Figure 2, which randomly generated by using the "peaks" function in MATLAB, x_phase $= a \cdot \text{peaks}(N)$. Figure 2(a) is the simulated noise-free ideal phase. With the Gaussian noise added, the corrupted phase is shown in Figure 2(b) and the signal-to-noise ratio SNR $= -1.406$dB. Filtered phases by using Goldstein, NL-InSAR and the SURE-based nonlocal method are illustrated in the second row of Figure 2(c)-(e), respectively.

From the coarse view of these figures, it is obvious that the noise is well suppressed especially by using the SURE-based nonlocal method, which can also be observed from the phase differences presented in the third row of Figure 2. Here the phase difference is measured between the filtered phase and the noise-free phase. In Figure 2(e), the phase difference values of most pixels are close to zero, which means that the filtered phase by using the SURE-based nonlocal method is more similar to the noise-free phase. Besides, the phase fringe continuity can be used to assess the noise reduction performance. The more continuous the fringes in the filtered phase, the better the performance of InSAR phase noise reduction. In the Goldstein and NL-InSAR filtered phase figures, the fringe patterns become discontinuous, such as some spike-like fringes generated in the highlighted regions within the white rectangles. And these discontinuous fringe patterns can also be observed from the phase difference maps.

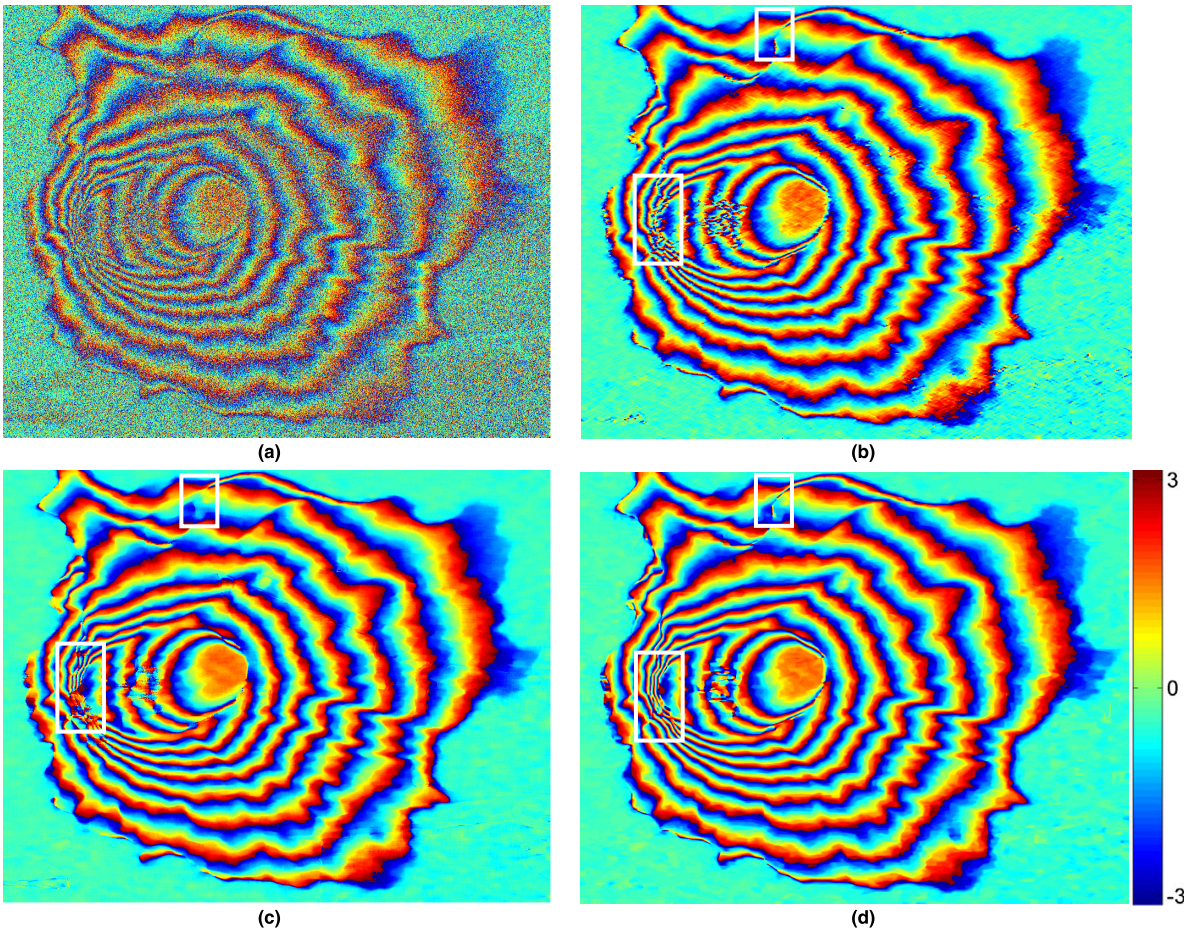

FIGURE 3. (a) Simulated noisy wrapped phase of the volcano. (b) Goldstein filtered phase. (c) NL-InSAR filtered phase. (d) Filtered phase using the improved SURE-based nonlocal method.

TABLE 1. Comparison of quantitative indexes for the simulated data.

	NOR	SNR	MSE	MSSIM
Noisy interferogram	56850	-1.4060	1.3645	0.0708
Goldstein	590	1.5041	0.2817	0.3578
NL-InSAR	576	4.0901	0.1068	0.5086
Proposed method	12	7.2192	0.0169	0.7480

In terms of evaluation, several quantitative indexes are used except for the visual inspection. The first index is the number of residues (NOR), which is estimated and given in Table 1. The NOR in the filtered interferogram is the commonly used metric to evaluate the effectiveness of phase noise reduction methods, and usually a small NOR indicates good filtering performance. In Table 1, the NOR with the SURE-based nonlocal method is 12 which is the smallest. Another widely used metric index is the SNR. The SNRs of the three filtered phases related to the noise-free phase are 1.5041, 4.0901 and 7.2192 respectively, which indicates that the SURE-based nonlocal method shows superiority to the other two filters when it comes to the filtered phase. And the running times of the three filters are 58s, 612s and 109s, respectively. Although the time cost of the proposed filter is more than it of Goldstein filter, but greatly deduced comparing to the NL-InSAR filter.

For the simulated data, a metric to assess the overfiltering in the noise reduction problem is the MSE between the filtered phase φ and the noise-free ideal phase φ_{ideal}. The MSE for the wrapped phase is defined as

$$\text{MSE} = E\left[\left|\arg\exp(j\varphi - j\varphi_{\text{ideal}})\right|^2\right] \tag{11}$$

where $\arg(\cdot) \in [-\pi, \pi]$ is the argument of the complex variable.

The smaller the MSE, the better the performance of the phase reduction. And the MSE values of the three filtered phase results are also given in Table 1 for comparison. Still, the SURE-based nonlocal method can achieve a smaller MSE value comparing to the other two filters. Since MSE is not well matched to the perceived visual quality based on the pointwise signal differences, the structure similarity (SSIM) map [8] is utilized for evaluation, which takes the advantages of known characteristics of human visual and considers image degradations as perceived changes in structural information variations. The form of the SSIM index are calculated within

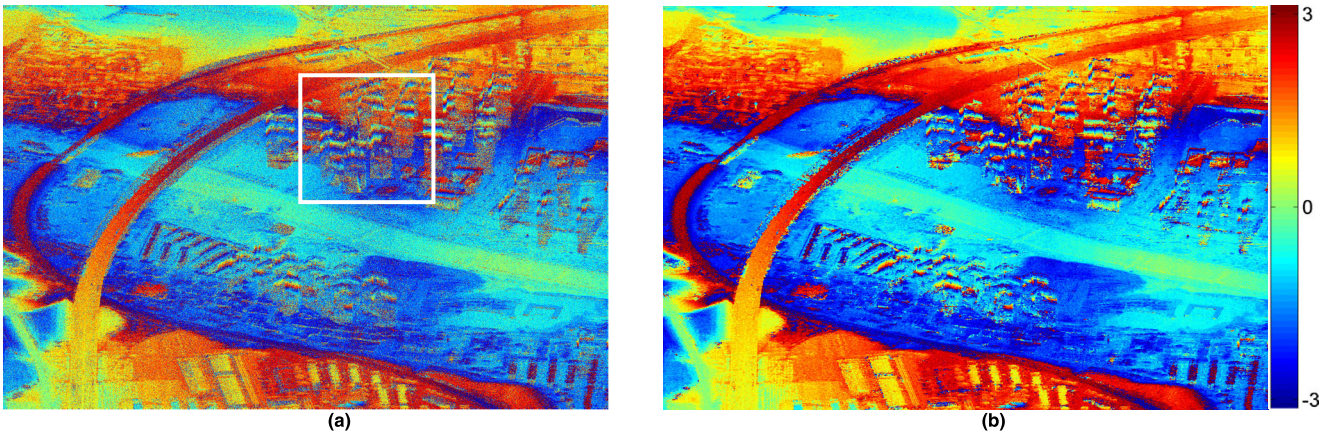

FIGURE 4. (a) InSAR phase of the real urban scene from Chinese N-SAR system. (b) Filtered phase using the improved SURE-based nonlocal method.

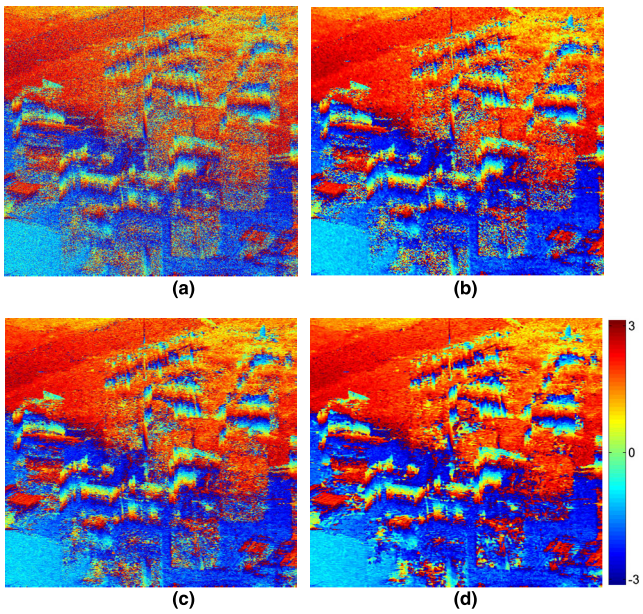

FIGURE 5. (a) Zoomed-in area in Figure 4(a). (b) Goldstein filtered result. (c) NL-InSAR filtered result. (d) SURE-based nonlocal filtered result.

the local window as the following expression

$$\mathrm{SSIM}(\mathbf{x},\mathbf{y}) = \frac{\left(2\mu_x\mu_y + C_1\right)\left(2\sigma_{xy} + C_2\right)}{\left(\mu_x^2 + \mu_y^2 + C_1\right)\left(\sigma_x^2 + \sigma_y^2 + C_2\right)} \tag{12}$$

where μ_x and μ_y represent the mean value of $\mathbf{x}$ and $\mathbf{y}$, respectively. And σ_x and σ_y are the unbiased estimates. C_1 and C_2 are the constants relating to the dynamic range, and $C_3 = C_2/2$.

In practice, one usually requires a single overall quality measure of the entire image, a mean SSIM (MSSIM) index [8] is calculated as Equation (13) and displayed in Table 1.

$$\mathrm{MSSIM}(\mathbf{X},\mathbf{Y}) = \frac{1}{M}\sum_{m=1}^{M}\mathrm{SSIM}(\mathbf{x}_m,\mathbf{y}_m) \tag{13}$$

where $\mathbf{X}$ and $\mathbf{Y}$ are the reference image and the distorted image, respectively. $\mathbf{x}_m$ and $\mathbf{y}_m$ are the image contents at the mth local window, and M is the number of local windows of the image.

The SURE-based nonlocal method can supply a much bigger MSSIM value comparing to the other two filters. And the SSIM maps to analyze the details preservation are illustrated in the last row of Figure 2. The SSIM index value is distributed in the interval [-1, 1], with 1 representing the best quality and -1 the worst. Apparently, the proposed method exhibits a significant advantage over the other two filters because there are significantly more pixels with SSIM value nearly to 1.

B. SIMULATED VOLCANO INTERFEROGRAM

Another simulated data of Etna Volcano is experimented to validate the proposed method. The noisy wrapped phase is shown in Figure 3(a). And the filtered results using Goldstein, NL-InSAR and the proposed method are illustrated in Figure 3(b), (c) and (d).

From the vision, the noise in the phase image is quite well suppressed by using SURE-based nonlocal method, and NL-InSAR filtered result appears a little better than Goldstein filtered result. And in the lower highlighted regions within the white rectangles, the fringe patterns again appear not continuous but spike-like noises in the filtered phase using the Goldstein and NL-InSAR filters. From the coarse view of the detail preservation in the up marked regions, the NL-InSAR seems a little oversmoothing and losts the structure details comparing to the others, viz. the fringe patterns are destroyed. The time costs are illustrated in Table 2. Still, the proposed filter is prior to NL-InSAR filter.

For quantitative analysis, except the NOR, another metric to evaluate the noise reduction performance is used which is the peak signal-to-noise ratio (PSNR) as follows [4]

$$\mathrm{PSNR} = 10\log_{10}\frac{4N_s\pi^2}{\left\|\mathcal{W}\left(\hat{\varphi}_{2\pi} - \varphi_{2\pi}\right)\right\|} \tag{14}$$

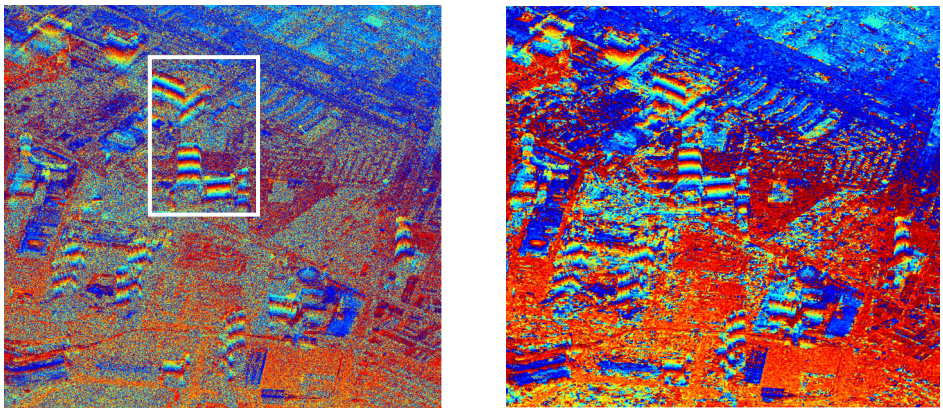

(a) (b)

FIGURE 6. (a) Real urban data from TanDEM-X. (b) Filtered phase using the improved SURE-based nonlocal method.

TABLE 2. Comparison of metric indexes for the simulated volcano data.

	NOR	PSNR	CC	TIME (s)
Noisy interferogram	342718			
Goldstein	992	58.2010	0.2568	209
NL-InSAR	616	58.2347	0.2540	2513
Proposed method	460	58.1958	0.2576	458

where N_s denotes the number of pixels, $\hat{\varphi}_{2\pi}$ and $\varphi_{2\pi}$ denotes the estimated wrapped phase and the true wrapped phase, respectively. And Ω is the wrapping operator.

And the higher the PSNR, the more the InSAR noise reduction. And the PSNRs of the three filter are nearly equivalent. For further analysis on details preservation, the correlation coefficients (CC) [8] between the original phase and the filtered phase are listed in Table 2, together with other two indexes.

When a filter is applied to an interferometric phase, we can also say that the phase is changed that noise is suppressed while details are inevitably removed. The degree of the change could be measured by means of CC and the performance of noise suppression could be indicated by the NOR values, and then the ability of details preservation could be inferred accordingly. It could be observed that more details are preserved in the image employing the SURE-based nonlocal method, because the estimated CC value of it is the biggest in Table 2, while its NOR is the smallest.

C. REAL URBAN DATA SETS

In this section, to test the filtering method on real urban data, two wrapped InSAR phase data sets of the wide scene are utilized. The first urban scene in Figure 4(a) is collected from Weinan City in China by the Chinese airborne N-SAR system [3].

In the wrapped phase image, the fringe pattern of the high-rise building layover is the prominent characteristic, which has already been used for urban building information extraction and reconstruction [3, 12]. Meanwhile, it is obvious that there are strong noises in the real phase image of this urban scene. In this scene, there are different terrain types including all kinds of buildings, motorway, trafficway, small bridge and so on. After filtering with the SURE-based nonlocal method, the InSAR phase of the wide scene is shown as Figure 4(b). The phase of the homogenous areas become smooth, and the fringe patterns in the high-rise areas become quite apparent.

To focus on the wrapped phase fringe patterns, the zoomed-in high-rise area in Figure 4(a) is highlighted in Figure 5(a). The filtered results of this high-rise area by using Goldstein filter, NL-InSAR filter and the proposed method are shown in Figure 5(b), (c) and (d). To avoid overfiltering and to keep the fringe patterns, the window sizes used in the three filters for the real urban data sets are all smaller than these for the simulate data sets. In Figure 5(b)-(d), the fringe patterns of high-rise building layover become quite apparent as the noise have been strongly suppressed. From the vision, the filtered results for homogenous area by using Goldstein filter and the proposed method are prior to NL-InSAR filtered result. And in the high-rise building layover, less dot-like noises still exist in Figure 5(d) comparing to Figure (b) and (c).

TABLE 3. Comparison of quantitative indexes for airborne N-SAR data.

	NOR	PSNR	CC	TIME(S)
Noisy interferogram	108270			
Goldstein	20154	58.7084	0.5477	145
NL-InSAR	37960	58.6233	0.6431	1530
Ours	3970	60.0180	0.5463	273

Meanwhile, the three metric indexes for quantitative evaluation are listed in Table 3. The time costs are also illustrated in Table 3. Obviously, the running times of the proposed filter deduced greatly comparing to NL-InSAR filter. The NOR of Figure 5(d) is the smallest, indicating less noise rest in Figure 5(d). And the same conclusion can be achieved as the PSNR of Figure 5(d) is the biggest. However, the

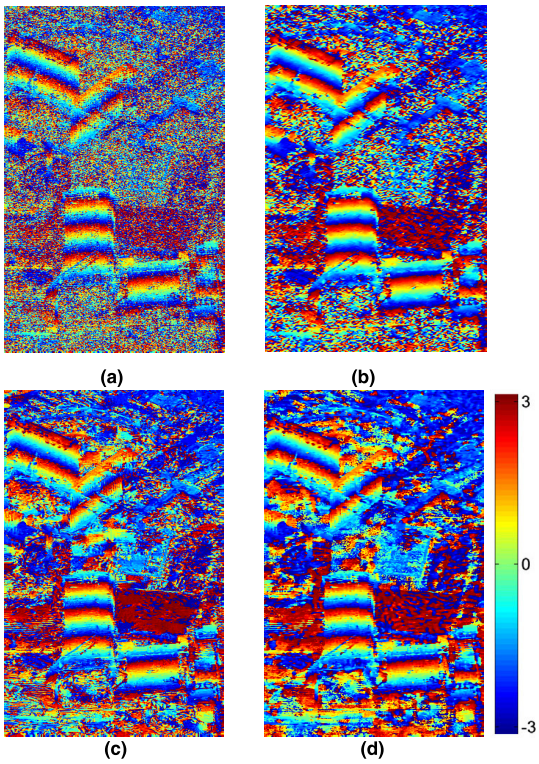

FIGURE 7. (a) Zoomed-in area in Figure 6(a). (b) Goldstein filtered result. (c) NL-InSAR filtered result. (d) SURE-based nonlocal filtered result.

estimated CC value of the proposed method is not the biggest, due to less dot-like noise kept in Figure 5(d). Hence, the CC value is not adopted for the next real urban data set.

Another urban scene data in Figure 6(a) is the wrapped interferometric phase of Las Vegas collected by TanDEM-X system [23]. There are also all types of buildings in this urban scene. Still, the strong noise covers on the fringe patterns of high-rise building layover. Before extracting the fringe pattern characteristic, the wrapped phase should be denoised and the filtered result by using the proposed method is shown as Figure 6(b). Again, the zoomed-in high-rise area in Figure 6(a) is highlighted in Figure 7(a). The filtered results of this high-rise area by using Goldstein filter, NL-InSAR filter and the proposed method are shown in Figure 7(b), (c) and (d). From the vision, the filtered results for homogenous area by using NL-InSAR and the proposed method are prior to Goldstein filtered result, as in the Goldstein filtered phase image the homogenous area seems not smooth. The NORs of the four figures in Figure 7 are 36854, 8980, 11614 and 3330, respectively. And then the PSNRs are 52.5381, 53.2379 and 52.6179 according to Figure 7(b)-(d). Hence, the proposed method can be used for the wide scene with all terrain types. Meanwhile, the running times of the three filters on this area are 69s, 711s, and 128s, respectively.

V. CONCLUSIONS

This paper focused on the interferometric phase filtering, for the InSAR phase contains most useful information of the observed terrain targets and has been applied in many remote sensing applications. In the paper, the SURE-based nonlocal mean has been investigated and improved for only InSAR phase denoising. Considering the fringe patterns in the InSAR phase image, the InSAR phase has been converted into the real and imaginary parts in the complex domain. Then the proposed filtering method deals with each part by using the SURE-based nonlocal means with the filtering parameters. After SURE map smoothing, the minimum SURE value is taken as the denoised result from the vectorization expression for each pixel. Finally the filtered phase is composed by the denoised real and imaginary parts. By taking the advantages of both the nonlocal means and the Stein's unbiased risk estimate, the proposed method can filter the noisy InSAR phase well while keeping more useful details including the fringe pattern. The experimental results of both the simulated data sets and two urban scene data sets validate the efficiency of the proposed InSAR phase filtering method on noise reduction and fringe pattern preservation.

REFERENCES

[1] G. Baier, C. Rossi, M. Lachaise, X. X. Zhu, and R. Bamler, "A nonlocal InSAR filter for high-resolution DEM generation from TanDEM-X interferograms," *IEEE Trans. Geosci. Remote Sens.*, vol. 56, no. 11, pp. 6469–6483, Nov. 2018.

[2] C. Dubois, A. Thiele, and S. Hinz, "Building detection and building parameter retrieval in InSAR phase images," *ISPRS J. Photogramm. Remote Sens.*, vol. 114, pp. 228–241, Apr. 2016.

[3] R. Guo, F. Wang, B. Zang, G. Jing, and M. Xing, "High-rise building 3D reconstruction with the wrapped interferometric phase," *Sensors*, vol. 19, no. 6, pp. 1439–1453, 2019.

[4] L. Otmar, N. Holger, K. Stefan, and Y. Wang, "Phase unwrapping for SAR interferometry—A data fusion approach by Kalman filtering," *IEEE Trans. Geosci. Remote Sens.*, vol. 46, no. 1, pp. 47–58, Jan. 2008.

[5] J. J. Martinez-Espla, T. Martinez-Marin, and J. M. Lopez-Sanchez, "A particle filter approach for InSAR phase filtering and unwrapping," *IEEE Trans. Geosci. Remote Sens.*, vol. 47, no. 4, pp. 1197–1211, Feb. 2009.

[6] J.-S. Lee, K. P. Papathanassiou, T. L. Ainsworth, M. R. Grunes, and A. Reigber, "A new technique for noise filtering of SAR interferometric phase images," *IEEE Trans. Geosci. Remote Sens.*, vol. 36, no. 5, pp. 1456–1465, Sep. 1998.

[7] G. Xu, M.-D. Xing, X.-G. Xia, L. Zhang, Y.-Y. Liu, and Z. Bao, "Sparse regularization of interferometric phase and amplitude for InSAR image formation based on Bayesian representation," *IEEE Trans. Geosci. Remote Sens.*, vol. 53, no. 4, pp. 2123–2136, Apr. 2015.

[8] Y. Wang, H. Huang, Z. Dong, and M. Wu, "Modified patch-based locally optimal Wiener method for interferometric SAR phase filtering," *ISPRS J. Photogramm. Remote Sens.*, vol. 114, pp. 10–23, Apr. 2016.

[9] R. M. Goldstein and C. L. Werner, "Radar interferogram filtering for geophysical applications," *Geophys. Res. Lett.*, vol. 25, no. 21, pp. 4035–4038, Nov. 1998.

[10] R. Chen, W. Yu, R. Wang, G. Liu, and Y. Shao, "Interferometric phase denoising by pyramid nonlocal means filter," *IEEE Geosci. Remote Sens. Lett.*, vol. 10, no. 4, pp. 826–830, Jul. 2013.

[11] Q. Wang, H. Huang, A. Yu, and Z. Dong, "An efficient and adaptive approach for noise filtering of SAR interferometric phase images," *IEEE Geosci. Remote Sens. Lett.*, vol. 8, no. 6, pp. 1140–1144, Nov. 2011.

[12] J. Zhu, X. Ding, Z. Li, J. Zhu, and B. Xu, "High-rise building layover exploitation with non-local frequency estimation in SAR interferograms," *Remote Sens.*, vol. 9, no. 6, p. 579, 2017.

[13] A. Buades, B. Coll, and J.-M. Morel, "Nonlocal image and movie denoising," *Int. J. Comput. Vis.*, vol. 76, no. 2, pp. 123–139, Feb. 2008.

[14] D. Van De Ville and M. Kocher, "SURE-based non-local means," *IEEE Signal Process. Lett.*, vol. 16, no. 11, pp. 973–976, Nov. 2009.

[15] D. Van De Ville and M. Kocher, "Nonlocal means with dimensionality reduction and SURE-based parameter selection," *IEEE Trans. Image Process.*, vol. 20, no. 9, pp. 2683–2690, Sep. 2011.

[16] C.-A. Deledalle, L. Denis, and F. Tupin, "NL-InSAR: Nonlocal interferogram estimation," *IEEE Trans. Geosci. Remote Sens.*, vol. 49, no. 4, pp. 1441–1452, Apr. 2011.
[17] J.-W. Li, Z.-F. Li, Z. Bao, Y.-L. Hou, and Z.-Y. Suo, "Noise filtering of high-resolution interferograms over vegetation and urban areas with a refined nonlocal filter," *IEEE Geosci. Remote Sens. Lett.*, vol. 12, no. 1, pp. 77–81, Jan. 2015.
[18] F. Luisier, T. Blu, and M. Unser, "Image denoising in mixed Poisson–Gaussian noise," *IEEE Trans. Image Process.*, vol. 20, no. 3, pp. 696–708, Mar. 2011.
[19] T. Qiu, A. Wang, N. Yu, and A. Song, "LLSURE: Local linear SURE-based edge-preserving image filtering," *IEEE Trans. Image Process.*, vol. 22, no. 1, pp. 80–90, Jan. 2013.
[20] C. Lopez-Martinez and X. Fabregas, "Modeling and reduction of SAR interferometric phase noise in the wavelet domain," *IEEE Trans. Geosci. Remote Sens.*, vol. 40, no. 12, pp. 2553–2566, Dec. 2002.
[21] J. Hu, R. Guo, X. X. Zhu, G. Baier, and Y. Wang, "Non-local means filter for polarimetric SAR speckle reduction-experiments using Terrasar-X data," in *Proc. ISPRS Ann. Photogramme., Remote Sens. Spatial Inform. Scien.*, Munich, Germany, Jun. 2015, pp. 71–77.
[22] V. Duval, F. Aujol, and Y. Gousseau, "On the parameter choice for the non-local means," HAL, Bengaluru, India, Tech. Rep. HAL-00468856, 2010.
[23] R. Guo and X. X. Zhu, "High-rise building feature extraction using high resolution spotlight TanDEM-X data," in *Proc. 10th EUSAR Conf.*, Berlin, Germany, Jun. 2014, pp. 1–4.

RUI GUO received the B.S. and Ph.D. degrees in electronic engineering from Xidian University, Xi'an, China, in 2007 and 2012, respectively. From 2012 to 2014, she was a full-time Postdoctoral Research Fellow with the German Aerospace Center (DLR), Remote Sensing Technology Institute. She is currently an Associate Professor with the School of Automation, Northwestern Polytechnical University. Her research interests include polarimetric/interferometric SAR imaging and application in remote sensing.

BO ZANG received the B.S. degree in electromechanical engineering and the Ph.D. degree in electronic engineering from Xidian University, Xi'an, China, in 2006 and 2011, respectively. He is currently a Lecturer with the School of Electronic Engineering, Xidian University. His research interests include inverse synthetic aperture radar (SAR) and lidar imaging.

SHUANG-XI ZHANG (Member, IEEE) received the B.S. degree in measuring control and instrument engineering and the Ph.D. degree in electronic engineering from Xidian University, Xi'an, China, in 2008 and 2014, respectively. He was a Research Fellow with the National University of Singapore (NUS), from 2014 to 2016. He is currently an Associate Professor with the School of Electronics and Information, Northwestern Polytechnical University. His research interests include SAR imaging, SAR interference, array signal processing, and electronicmagnetic scattering.

MENG-DAO XING (Member, IEEE) received the B.S. and Ph.D. degrees in electronic engineering from Xidian University, Xi'an, China, in 1997 and 2002, respectively. He is currently a Full Professor with the National Laboratory of Radar Signal Processing, Xidian University. He holds the appointment of an Associate Dean with the Academy of Advanced Interdisciplinary Research. He has authored or coauthored two books and over 200 articles. His research interests include SAR, ISAR, sparse signal processing, and microwave remote sensing.